Dual-Stage Vertical Feedback for High-Speed Scanning Probe Microscopy

Andrew J. Fleming

***Abstract*—Many popular modes of scanning probe microscopy require a vertical feedback system to regulate the tip-sample interaction. Examples include constant-current scanning tunneling microscopy and constant-force atomic force microscopy. Due to the control of tip-sample interaction, these modes of microscopy provide precise topographic information and result in drastically reduced sample damage, hence their popularity. Unfortunately the vertical feedback controller also imposes a severe limit on the scan-speed of scanning probe microscopes. In this paper, the foremost bandwidth limitation is identified to be the low-frequency mechanical resonances of the scanner. To overcome this limitation, a dual-stage vertical positioner is proposed. This comprises the original scanner, plus an additional high-speed stage. The improved bandwidth provided by the high-speed stage allows a vast improvement in feedback gain and bandwidth. In this work, the bandwidth is increased from 83 Hz to 2.7 kHz. This improvement allows image quality to be retained with a speed increase of 33 times, or alternatively, feedback error can be reduced by 33 times if scan speed is not increased. The techniques proposed are mechanically and electrically simple and can be retrofitted to any scanning probe microscope.**

***Index Terms*—Atomic force microscopy, dual-stage, high-speed.**

I. Introduction

SINCE THE invention of the scanning tunneling microscope in 1981 [1] and the atomic force microscope in 1986 [2], scanning probe microscopes (SPMs) have revolutionized the imaging and manipulation of materials at the molecular and atomic scale [3].

The fundamental operation of an SPM is to scan a probe over a surface and map the interactions that occur as a function of location. In addition to topographic imaging, SPM probes have diversified to allow the mapping of a wide range of electrical, mechanical, chemical, biological, and physical interactions [4]–[8].

One of the foremost weaknesses of a scanning probe microscopes is the slow speed at which images are recorded. Standard commercial microscopes scan at speeds of typically 1 to 10 lines per second, so a single image may take minutes to acquire. Although in many applications the slow imaging time is simply an inconvenience, in other applications, this becomes a critical limitation. Examples where speed is a primary concern include: large-range surface inspection [9], [10], nanofabrication [11]–[14], and imaging of fast biological and physical processes [15]–[20].

There are three main limitations to the speed of a scanning probe microscope: 1) the resonance frequency or bandwidth of the probe [21]; 2) the mechanical bandwidth of the lateral positioner (scanner) [18], [22]–[24]; and 3) the bandwidth of the vertical positioner and feedback system, [18], [24].

Extensive research on the design and control of scanning probe microscopes has been motivated by these limitations. Recent reviews of this research can be found in references [25]–[28]. Many different techniques have been proposed to address point 1). These include self actuating cantilevers [29], active cantilever Q control [30], and short, high-speed cantilevers with resonance frequencies over 1 MHz [24], [31]. Of all the techniques available, the new generation of shorter cantilevers is deemed most suitable for high-speed AFM [24]. Such devices are now becoming commercially available with extremely high resonance frequencies and low-spring constants for both contact and tapping-mode AFM, for example, the Olympus Biolever series.

In recent years, considerable improvements have also been made to the mechanical bandwidth of the lateral positioning scanner [22], [23]. The greatest speed increases have resulted from completely new mechanical designs, such as [17]–[20], [24], [32]. However, such designs necessarily require small samples sizes and have low scan ranges. These factors can preclude the use of such techniques in general purpose applications. Alternatively, more moderate but still substantial speed increases have also been achieved by better control of existing hardware. With an accurate model, more aggressive controllers can achieve a ten times improvement in scan speed. Such techniques include: actuator linearization [22], [33], [34], feedforward control and input shaping [22], [35], and improved feedback control [18], [22]–[24].

The final remaining speed limitation of a scanning probe microscope is the vertical feedback bandwidth [18], [24]–[26]. That is, the bandwidth of the control loop that maintains a constant force interaction between the probe and sample. This topic is discussed in detail in Section III. Although some imaging modes do not require vertical feedback, for example constant-height mode, these are used only in applications where the sample is extremely flat and immune to probe damage.

Manuscript received June 23, 2009. Manuscript received in final form January 05, 2010. First published February 17, 2010; current version published December 22, 2010. Recommended by Associate Editor S. Devasia. This work was supported by the Australian Research Council (DP0666620) and the Centre for Complex Dynamic Systems and Control. Experiments were conducted at the Laboratory for Dynamics and Control of Nanosystems, University of Newcastle.

The author is with the School of Electrical Engineering and Computer Science, The University of Newcastle, Callaghan, NSW 2308, Australia (e-mail: andrew.fleming@newcastle.edu.au).

Color versions of one or more of the figures in this paper are available online at http://ieeexplore.ieee.org.

Digital Object Identifier 10.1109/TCST.2010.2040282

The foremost bandwidth limitation of the vertical feedback loop is typically the vertical positioner resonance. In commercial microscopes, vertical and lateral positioning is usually performed by a single device, commonly a piezoelectric tube scanner. A drawback is that low-frequency lateral resonances are coupled into the vertical dynamics. To combat this limitation, a number of approaches have been proposed that either improve the resonance frequency of the vertical positioner or eliminate it from the feedback loop. All of the high-speed microscope designs incorporate scanners with high vertical resonance frequencies, typically above 100 kHz [16]–[20]. Other designs that eliminate scanner dynamics from the feedback loop include piezoelectric actuated probes [36], magnetically actuated probes [37], and electrostatically actuated probes [38].

Although all of these techniques are effective in their own right, there are drawbacks that limit the direct application in a standard microscope. The high-speed scanners require specially prepared small samples and have a limited range of only a few hundred nanometers [19], [20]. Other techniques require highly specialized probes and/or significant mechanical modifications. None can be applied directly to a standard scanning probe microscope without significant modification.

In this work, a piezoelectric stack actuator is used to provide high-speed vertical positioning. The stack actuator is combined with the microscopes own piezoelectric tube positioner to provide both large range and high resonance frequency in the vertical axis. In Section V, this approach is demonstrated to increase the resonance frequency of a commercial AFM from 680 Hz to 23 kHz. This allows an increase in closed-loop bandwidth from 83 Hz to 2.7 kHz. The increased bandwidth results in significant image quality improvements, particularly when scanning at large range or high speed. The dual-stage system presented in this paper is designed to be low-cost, easy to use, mechanically and electrically simple and compatible with all modes and types of scanning probe microscope.

The benefits of a dual-stage vertical feedback system have also been recognized by other authors [27], [39], [40]. In [39] a high-speed positioner is integrated into the scan head by the microscope manufacturer. Although this results in a convenient and compact solution, such an approach requires significant hardware modifications. In [40] and [27], a model-based controller is used in the vertical feedback loop. The benefits here are improved performance; however, this comes at the expense of simplicity and usability. The controller must be redesigned after a significant change in the cantilever or sample.

The objective of this paper is to demonstrate the improvements that can be achieved with a positioner and controller simple enough to be applicable to all modes and types of scanning probe microscopy. A speed increase of 33 times is demonstrated with a total hardware cost of less than \$100.

This paper continues with a description of the experimental apparatus in the following section. The dynamics and limitations of a standard vertical feedback loop are then discussed in Section III. A high-speed positioner is then introduced in Section IV and combined with the standard positioner in Section V. Imaging experiments and conclusions are presented in Sections VI and VII.

Fig. 1. NT-MDT Ntegra scanning probe microscope arranged in scan-by-probe configuration. The scan head is mounted above a stationary sample platform.

II. Experimental Setup

In this work, an NT-MDT Ntegra scanning probe microscope is used to demonstrate the proposed techniques. The scanner is an NT-MDT Z50309cl piezoelectric tube scanner with 100-μm lateral range and 10-μm vertical range. The scanner comprises two piezoelectric tubes joined at the base. One tube is used for lateral positioning, and the other for vertical positioning. The internal and external electrodes of the vertical positioner are driven with equal but opposite voltages.

A signal access module allows direct access to the cantilever deflection, scanner electrode voltages, and reference trajectory.

III. Vertical Feedback Dynamics

The vertical feedback control system for an atomic force microscope is pictured in Fig. 2(a). This microscope is operating in constant-force contact-mode. The piezoelectric tube scanner moves the probe in a vertical direction to regulate the cantilever deflection dfl to the set-point r. The cantilever deflection is measured in the standard way using a reflected laser beam and photodiode [26].

Although the diagram in Fig. 2(a) represents an AFM operating in constant-force contact-mode, the schematic is similar to all forms of SPM where the tip-sample interaction is controlled. The only difference between operating modes is the measured feedback variable. For example, in constant-force contact-mode AFM, the feedback variable is cantilever deflection, while in constant-current STM, the feedback variable is tunneling current. Other feedback variables include the cantilever oscillation magnitude in tapping-mode AFM and the fiber oscillation magnitude in scanning near-field optical microscopy. All of these modes share the same feedback system but with different feedback variables or methods of detection.

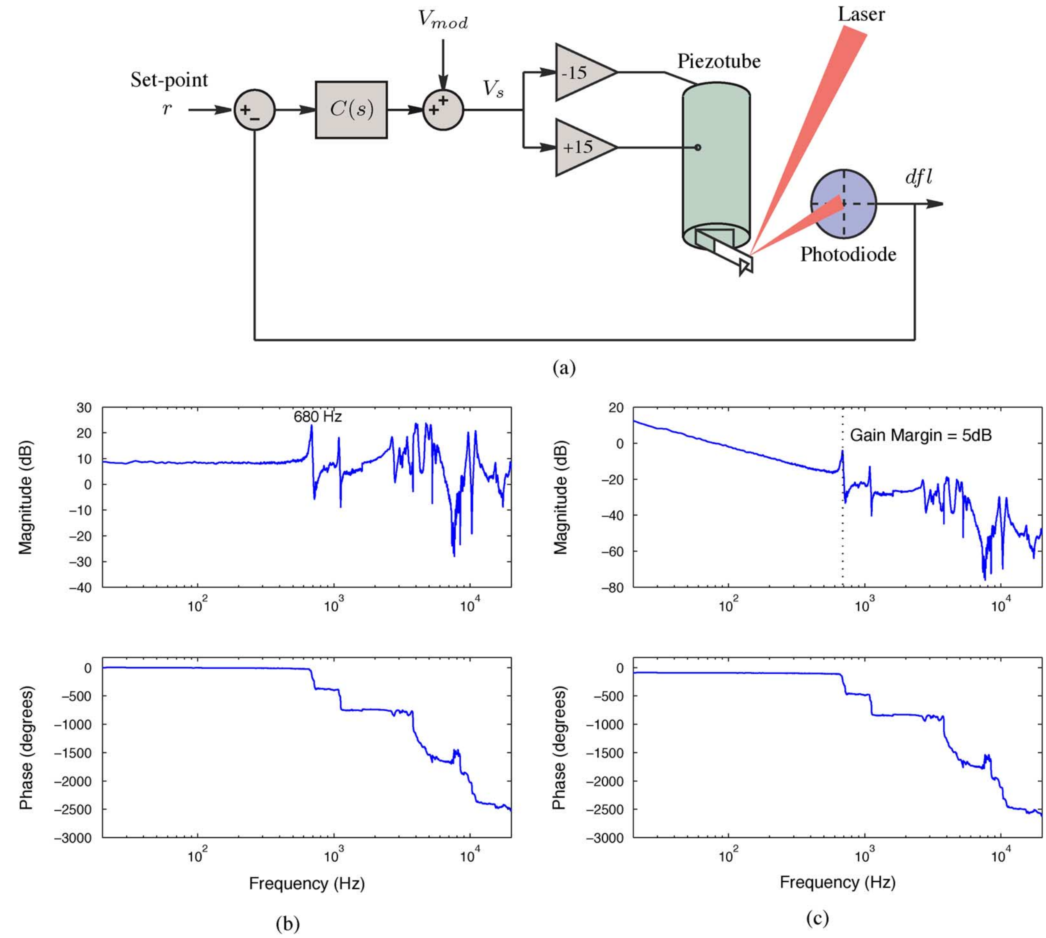

Fig. 2. ***Standard vertical feedback control system***. (a) Schematic diagram; (b) open-loop frequency response G_{dV_s} measured from the applied voltage V_s to the cantilever deflection dfl; (c) loop-gain of the vertical feedback loop with an integral controller of gain $\alpha = 190$. The closed-loop bandwidth is 83 Hz.

The vertical feedback control system in Fig. 2(a) comprises the set-point summing junction, the controller $C(s)$ and the driving amplifiers, which in this case are connected to the internal and external tube electrodes. The controller $C(s)$ is most commonly an integral controller, i.e.,

$$C(s) = \frac{\alpha}{s}. \tag{1}$$

Integral controllers are popular as they are simple to implement, provide good regulation of tip-sample interaction at low frequencies, and are easily adjustable. Ease of tuning is a necessity as the feedback system must accommodate multiple SPM modes and cope with a wide range of probes and samples.

From a control perspective, the plant under consideration consists of all dynamics between the control voltage V_s and the measured deflection dfl. This encompasses the amplifier dynamics, the scanner and cantilever mechanics and the tip-sample interaction. This system is denoted G_{dV_s}, where

$$G_{dV_s}(s) = \frac{dfl(s)}{V_s(s)}. \tag{2}$$

Although the system G_{dV_s} cannot be measured in open-loop, it is straightforward to do so in closed-loop. This is achieved by first approaching the probe to the sample described in Section VI, then drastically reducing the gain α until the controller only maintains the correct DC operating point. This maintains the probe-sample interaction during the frequency response. The frequency response of G_{dV_s} can then be measured directly by applying an excitation to V_{mod}. The experimental response of G_{dV_s} is plotted in Fig. 2(b). The response is essentially flat from dc to 680 Hz where the first resonance frequency of the scanner occurs. The resonance at 680 Hz is the first lateral bending mode of the scanner coupled into the vertical response. Following is the second lateral bending mode, then a dense collection of modes including torsional modes and the first piston mode [41].

From the frequency response in Fig. 2(b) it is clear that G_{dV_s} is an extremely complicated system. It contains the mechanical scanner dynamics, the tip-sample interaction and the dynamics of the driving and sensing electronics. However, from a control perspective, there are essentially only two important features: the dc sensitivity $G_{dV_s}(0)$ and the first resonance mode.

The dc sensitivity is a function of the amplifier gain, scanner sensitivity, cantilever geometry, sample stiffness, and detector sensitivity. All of these are constants except for the cantilever geometry and sample stiffness, which can vary widely. The variation in these parameters is the foremost reason that vertical feedback controllers must be retuned whenever a significant change in the cantilever or sample is made.

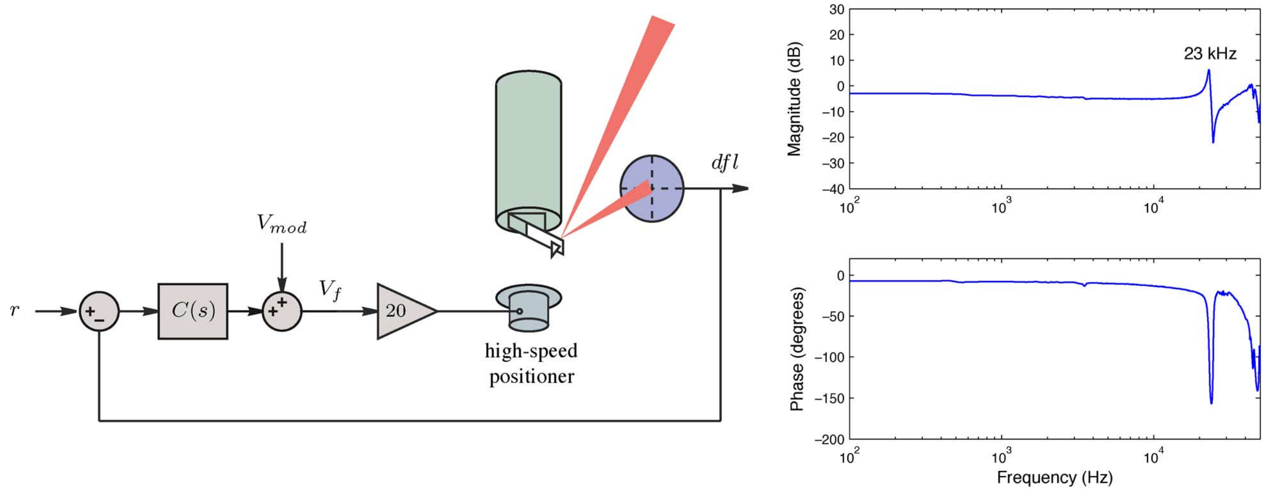

(a) (b)

Fig. 3. ***High-speed vertical feedback control system***. (a) Schematic diagram; (b) open-loop frequency response G_{dV_f} measured from the applied voltage V_f to the cantilever deflection dfl.

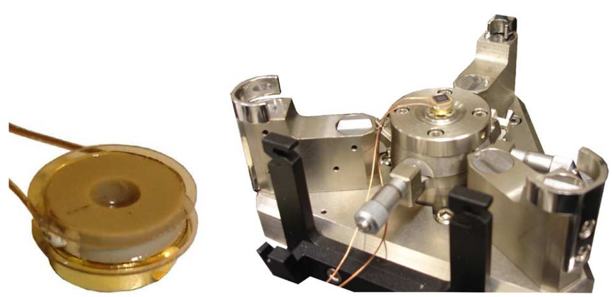

(a) (b)

Fig. 4. (a) High-speed vertical positioner (b) mounted on the microscope base with an attached sample.

While the dc sensitivity of G_{dV_s} is a function of many microscope properties, the lowest frequency dynamics of G_{dV_s} are the due to the lateral scanner resonances. Although the tip-sample interaction and cantilever dynamics are also important, these occur at much higher frequencies than the first scanner resonance and have little effect on the control performance. Instead, the maximum controller gain and closed-loop bandwidth are dependent on the resonance frequency and damping ratio of the first resonant mode. This can be understood by considering the frequency response of the controller loop-gain $C(s) \times G_{dV_s}(s)$ plotted in Fig. 2(c).

From the plot of loop-gain in Fig. 2(c), it is clear that the controller gain is limited by the low gain-margin imposed by the first mechanical resonance at 680 Hz. Due to the large phase drop at this frequency, the loop-gain must be less than 0 dB if the system is to be stable. The condition when this occurs is

$$PG_{dV_s}(0)\frac{\alpha}{\omega_1} < 1 \tag{3}$$

where P is the difference between the dc sensitivity $G_{dV_s}(0)$ and the peak magnitude of the first resonance mode and ω_1 is the first resonance frequency. P is easily measured in decibels from the magnitude frequency response. In Fig. 2(b), P is approximately 15 dB or 5.6. Note: If P is measured in dB, the value of P must be converted to linear magnitude by

$$P = 10^{P_{\mathrm{dB}}/20}. \tag{4}$$

Rather than simply a condition on stability, it is preferable to procure a condition that guarantees a certain amount of gain-margin, i.e., the additional gain that can be added to the loop before the system becomes unstable. As the sensitivity of piezoelectric actuators can increase by up to 100% with increases in bias voltage and temperature, the gain-margin should be chosen conservatively at approximately 2 or 6 dB. With the inclusion of gain-margin in the expression for maximum loop-gain, (3) becomes

$$PG_{dV_s}(0)\frac{\alpha}{\omega_1} < \frac{1}{\text{gain–margin}} \tag{5}$$

where gain-margin should be expressed as a linear quantity.

From the expression of maximum loop-gain in (5), the maximum controller gain $\alpha_{\max}$ can be derived

$$\alpha_{\max} < \frac{\omega_1}{PG_{dV_s}(0)} \times \frac{1}{\text{gain–margin}}. \tag{6}$$

That is, the controller gain can be increased if the first resonance frequency ω_1 is increased or the magnitude of the resonance peak is decreased. The controller gain can also be increased at the expense of gain-margin, however this is undesirable.

With an integral controller, the closed-loop transfer function can be approximated by

$$G_{cl}(s) = \frac{\alpha G_{dV_s}(0)}{s + \alpha G_{dV_s}(0)}. \tag{7}$$

The maximum closed-loop bandwidth of this system is approximately $\alpha_{\max} G_{dV_s}(0)$. If the expression for maximum controller gain (6) is substituted, the maximum closed-loop bandwidth can be found as a function of only the resonance frequency, peak magnitude and desired gain-margin

$$\boxed{\max.\text{bandwidth} = \tfrac{\omega_1}{P} \times \tfrac{1}{\text{gain–margin}},} \tag{8}$$

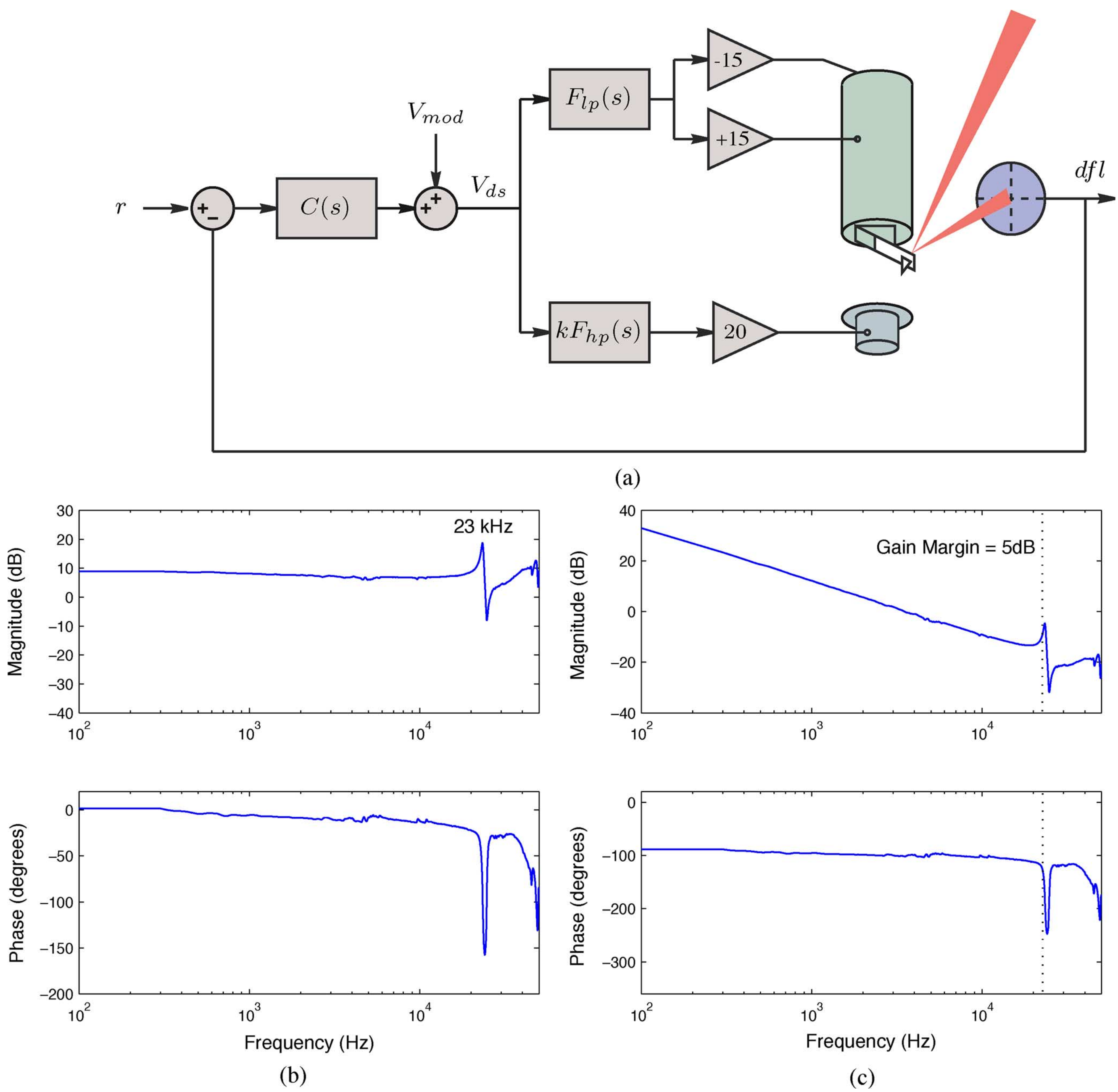

Fig. 5. ***Dual-stage vertical feedback control system***. (a) Schematic diagram; (b) open-loop frequency response of the dual-stage positioning stage $G_{\rm ds}$ measured from the dual-stage voltage V_{ds} to the cantilever deflection dfl; and (c) loop-gain of the dual-stage vertical feedback loop with an integral controller of gain $\alpha = 10\,000$. The closed-loop bandwidth is 2.7 kHz.

thus, for a fixed gain-margin, the maximum closed-loop bandwidth increases as the first resonance frequency ω_1 is increased or the magnitude of the resonance peak is decreased.

Considering the open-loop frequency response in Fig. 2(b) and (8), the maximum closed-loop bandwidth should be approximately $680/5.6 = 120$ Hz. With a gain-margin of 5 dB the estimated closed-loop bandwidth decreases to 68 Hz. This compares well to the experimental closed-loop bandwidth of 83 Hz. This value was determined from the closed-loop frequency response plotted in Fig. 7. The controller gain was $\alpha = 190$, which resulted in a gain-margin of 5 dB. The discrepancy between the estimated and measured closed-loop bandwidth is due to the large tolerance in capacitive components used to implement the analog controller.

The imaging consequences of the low vertical feedback bandwidth are discussed in Section VI.

IV. High-Speed Vertical Positioning

From the previous section, and in particular, from (8), it should be clear that the frequency of the first mechanical resonance determines the maximum closed-loop bandwidth of the vertical feedback system. Hence, to improve the closed-loop response, the first resonance frequency of the scanner must be increased.

With a tube scanner, the only practical method of increasing the resonance frequency is to reduce the tube dimensions. Tube length has the greatest effect on resonance frequency [42]; which is inversely proportional to the length squared [42]. Thus, a shorter tube has a significantly higher resonance frequency. However, the maximum lateral deflection is also proportional to the length squared [43], so any increase in resonance frequency is accompanied by a proportional decrease in scan range, which is highly undesirable. This tradeoff is summarized as follows:

$$\omega_1 \propto \frac{1}{L^2} \quad d_{\max} \propto L^2 \Rightarrow \omega_1 \propto \frac{1}{d_{\max}} \tag{9}$$

where L is the tube length and $d_{\max}$ is the maximum lateral deflection.

In addition to the detrimental tradeoff with scan range, it is also undesirable to modify the tube as this may required significant hardware modifications. These modifications may be difficult to implement, particularly in scan-by-probe systems where the scanner is tightly integrated with the optical and probe assemblies.

A better option than modifying the tube scanner is to replace it with a faster vertical positioner. The diagram of a high-speed vertical feedback system is pictured in Fig. 3(a). Here, the piezoelectric tube is no longer used for vertical positioning. A second, high-speed positioner drives the sample holder directly.

The high-speed positioner shown in Fig. 4 comprises a piezoelectric actuator and small magnet that is highly attracted to the microscope's magnetic base. A mica wafer is used for electrical isolation between the actuator and magnet, and also between the actuator and sample. The piezoelectric actuator is an 8-mm diameter multi-layer piezoelectric disk (CMAR02) manufactured by Noliac A/S, Denmark. This actuator is driven with a PiezoDrive PDL200 voltage amplifier.

The piezoelectric actuator is specified to develop a stroke of 2.7 μm at 200 V. However, as the base of the actuator is constrained, the stroke when bonded to the magnet reduces to approximately 1 μm. This is due to Poisson coupling which results in a lateral contraction when the actuator elongates. If the base is constrained, the actuator is not free to contract laterally which introduces a counteractive stress and consequently, a reduction in range. This effect becomes more significant in actuators with a small length compared to their lateral dimensions, i.e., short fat actuators, such as that used here.

An alternative to the configuration shown in Fig. 3(a) is to mount the high-speed positioner on the end of the tube scanner. However, in this configuration, the high-speed stage can excite low-frequency resonances of the tube scanner. In a scan-by-sample microscope, the high-speed positioner can be added to the sample scanner or the stationary probe holder.

The frequency response of the high-speed positioner is plotted in Fig. 3(b). The resonance frequency of 23 kHz is 33 times faster than the piezoelectric tube actuator. However, the penalty is a ten-fold reduction in range.

Although a 1-μm stroke is sufficient for most forms of scanning probe microscopy, it requires an approach mechanism with extremely fine resolution. In addition, larger samples or tilted samples may also require a greater stroke, up to a few microns in some cases. To alleviate the problem of low stroke, a dual-stage approach is described in the following section that achieves both wide range and fast response.

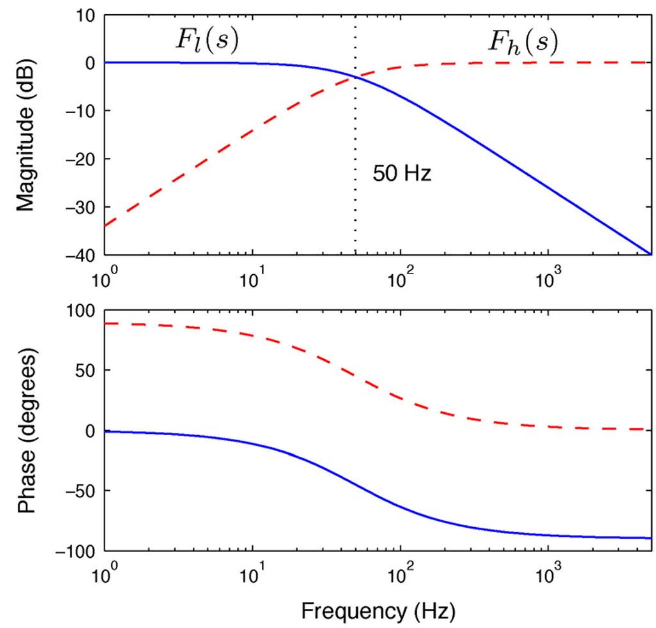

Fig. 6. Frequency response of the complimentary filters $F_{\mathrm{hp}}(s)$ and $F_{\mathrm{lp}}(s)$.

V. Dual-Stage Positioning

To facilitate probe landing and to compensate for thermal drift, a vertical positioning stroke of around 10 μm is required in general purpose microscopes. As the high-speed stage in the previous subsection only develops a 1-μm stroke, additional stroke is required from the tube scanner. The combined use of the high-speed positioner and piezoelectric tube is commonly referred to as a *dual-stage* actuator. The high-speed stage provides fast, short-range motions for imaging while the tube provides slower, long-range positioning for drift compensation and probe landing. This arrangement is illustrated in Fig. 5(a).

Although there are many techniques available for the control of dual stage systems [44], only a small subset are suitable in this application. Here, simplicity is a major consideration as the system must be easily retuned (with a single parameter) for different probe and sample combinations. In addition, simplicity is also required for analog implementation which is demanded by the bandwidth and noise requirements of the control-loop.

With these considerations in mind, one option is to simply utilize the two actuators in different frequency ranges. In Fig. 5(a) a pair of complementary high- and low-pass filters F_{hp} and F_{lp} are shown. As these filters are complementary, they sum to 1, i.e.,

$$F_{\mathrm{hp}} + F_{\mathrm{lp}} = 1. \tag{10}$$

A pair of complementary filters that are easy to implement with an analog circuit are

$$F_{\mathrm{hp}} = \frac{s}{s+\omega_c} \quad \text{and} \quad F_{\mathrm{lp}} = \frac{\omega_c}{s+\omega_c} \tag{11}$$

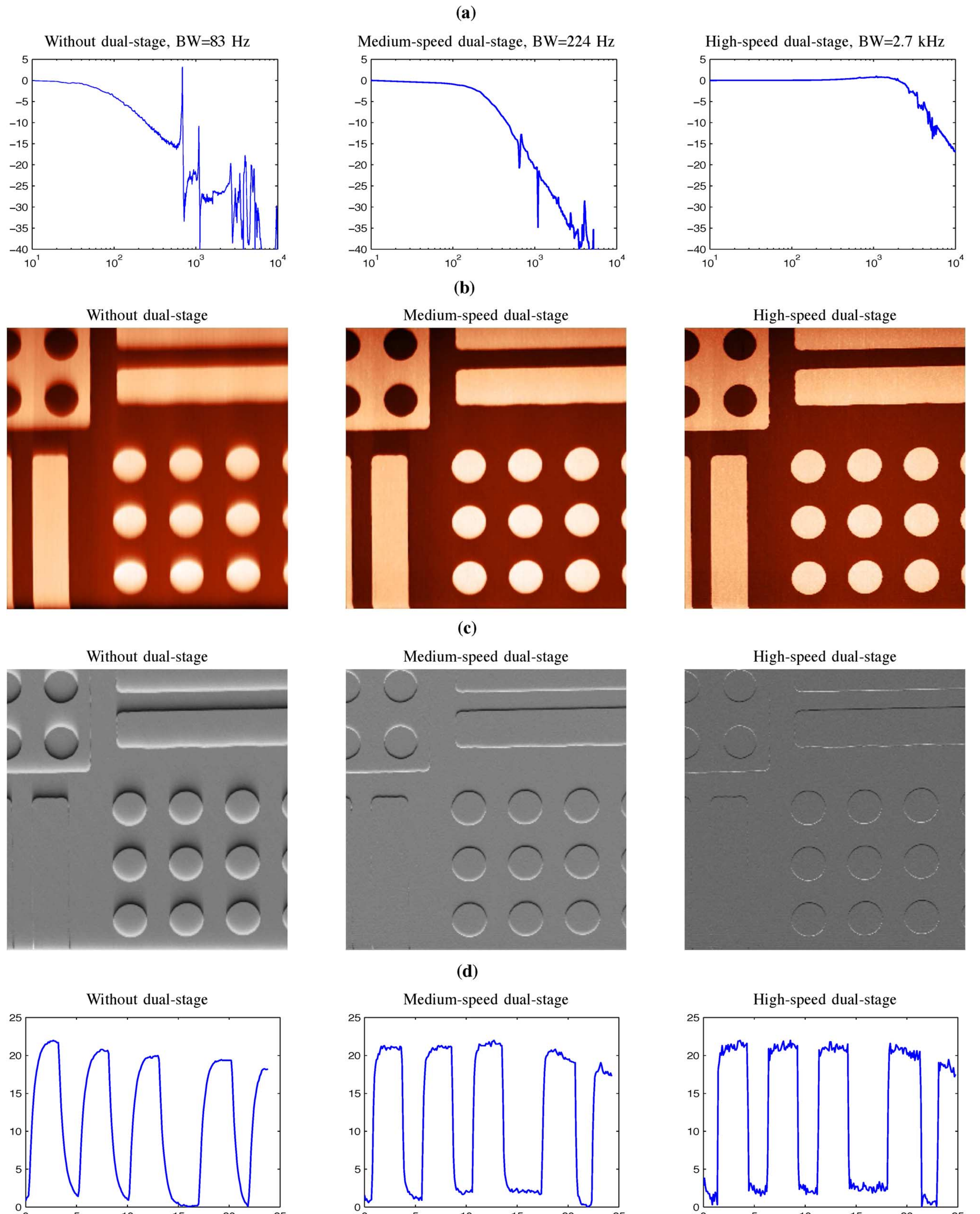

Fig. 7. Performance comparison of a standard vertical feedback controller with the medium-speed ($\alpha = 1000$) and high-speed ($\alpha = 10000$) dual-stage controller. The images were recorded at 2.84 Lines/s or 142 μm/s. (a) Force tracking transfer function (magnitude in decibels versus frequency in hertz) and tracking bandwidth; (b) 25×25 μm constant force images of a 20-nm feature height calibration standard, taken at 142 μm/s; (c) Cantilever deflection (force error); (d) Single image line, (vertical height in nanometers versus position in micrometers).

where ω_c is the cutoff frequency. The frequency response when $\omega_c = 2\pi 50$ is plotted in Fig. 6.

With the complementary filters installed, the dual-stage transfer function from the control voltage $V_{\rm ds}$ to the deflection

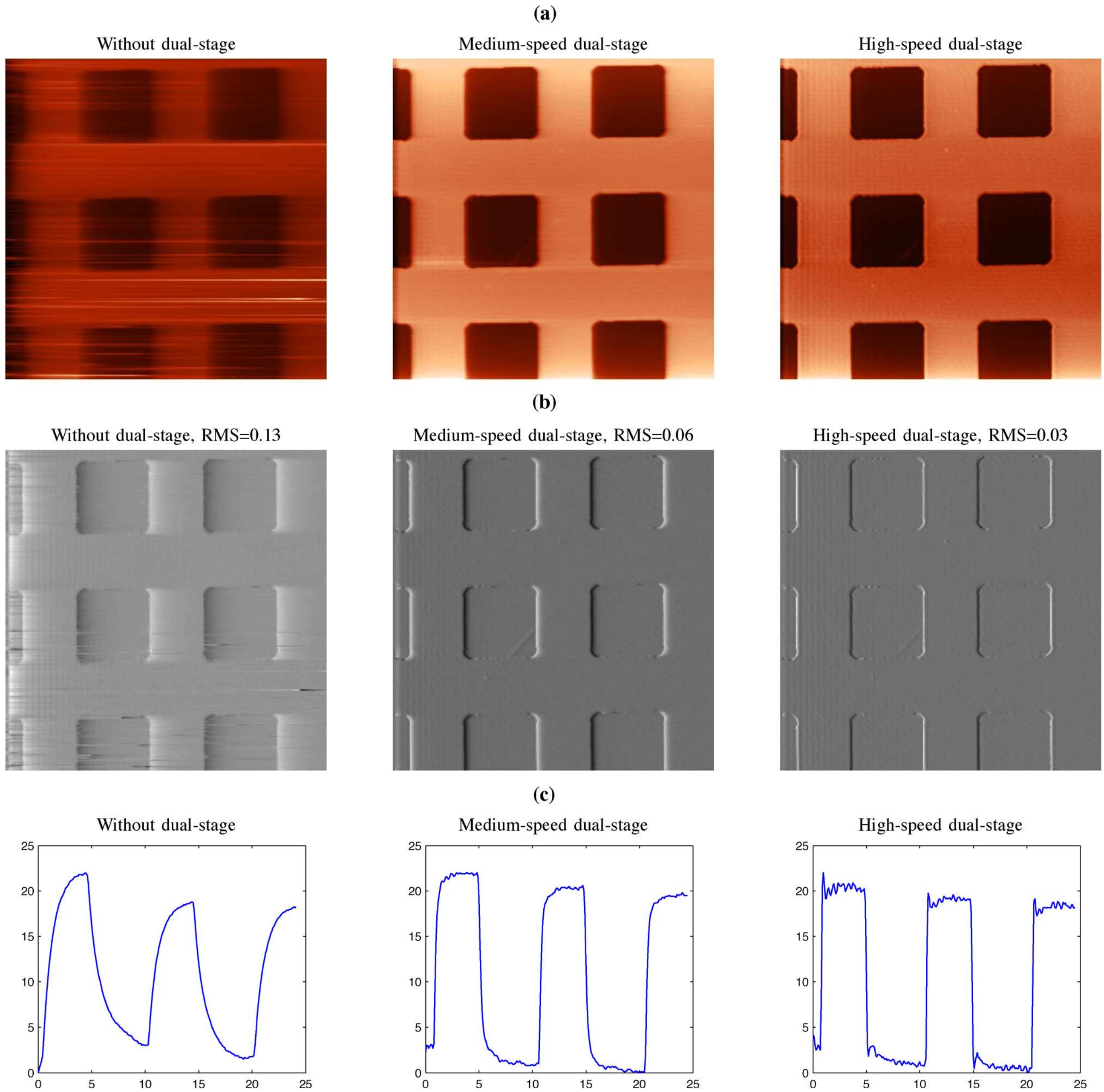

Fig. 8. Performance comparison of a standard vertical feedback controller with the medium-speed ($\alpha = 1000$) and high-speed ($\alpha = 10\,000$) dual-stage controller. The images were recorded at 6.25 lines/s or 312 μm/s. (a) 25 × 25 μm constant force images of a 20-nm feature height calibration standard, taken at 312 μm/s; (b) Cantilever deflection (force error) and RMS error; (c) Single image line, (vertical height in nanometers versus position in micrometers).

dfl, denoted G_{ds}, can be expressed as the sum of the slow and fast systems G_{dV_s} and G_{dV_f}, respectively

$$G_{\mathrm{ds}} = \frac{dfl}{V_{\mathrm{ds}}} \tag{12}$$
$$= kF_{\mathrm{hp}}G_{dV_f} + F_{\mathrm{lp}}G_{dV_s} \tag{13}$$

where k is the gain required to equate the sensitivity of G_{dV_f} to G_{dV_s}, i.e.,

$$k = \frac{G_{dV_s}(0)}{G_{dV_f}(0)}. \tag{14}$$

In Fig. 5(a) a gain of $k = 4.0$ is required to equate the sensitivity of the low- and high-frequency paths.

By setting the cutoff frequency ω_c one decade lower than the lowest resonance frequency of the piezoelectric tube, i.e., $\omega_c = 2\pi 50$, the product $F_{\mathrm{lp}}G_{dV_s}$ can be approximated by $F_{\mathrm{lp}}G_{dV_s}(0)$. Hence, the dual-stage transfer function G_{ds} can also be approximated by

$$G_{\mathrm{ds}} = kF_{\mathrm{hp}}G_{dV_f} + F_{\mathrm{lp}}G_{dV_s}(0) \tag{15}$$
$$= kF_{\mathrm{hp}}G_{dV_f} + F_{\mathrm{lp}}kG_{dV_f}(0) \tag{16}$$
$$= k(F_{\mathrm{hp}} + F_{\mathrm{lp}})G_{dV_f} \tag{17}$$
$$= kG_{dV_f}. \tag{18}$$

That is, the dual-stage transfer function has the sensitivity of the long-range piezoelectric tube and the bandwidth of the high-speed stage. The maximum high-frequency sample profile range is equal to the maximum stroke of the high-speed positioner, which is 1 μm. The frequency response of the dual-stage system is plotted in Fig. 5(b).

Due to the wide bandwidth of the dual-stage system, an integral controller with a gain of $\alpha = 10\,000$ can be applied directly while maintaining a gain-margin of 5 dB. The loop-gain with such a controller is plotted in Fig. 5(c). The improvement in closed-loop bandwidth and the corresponding imaging improvements are discussed in Section VI.

VI. Imaging Experiments

In this section, the imaging performance of the dual-stage system is compared to the standard feedback system described in Section III. Due to a resonance at 680 Hz, the standard feedback system is limited to a gain of $\alpha = 190$ which results in a closed-loop bandwidth of only 83 Hz. This will be compared to two dual-stage controllers, one with a gain of $\alpha = 1000$, and another with the maximum gain of $\alpha = 10000$. These controllers will be referred to as the medium-speed and high-speed dual-stage controller.

The closed-loop frequency response, from r to dfl, is plotted in Fig. 7(a). Clearly the dual-stage controllers provide a much wider and more regulated bandwidth. The maximum dual-stage bandwidth of 2.7 kHz is 33 times faster than the standard control system.

The effect of the improved bandwidth is demonstrated in Fig. 7(b) where a BudgetSensors HS-20MG calibration standard is imaged with an NT-MDT NSG03 cantilever (90 kHz, 0.5 N/m). The lower bandwidth controller "smears" the edges of the sample and filters small features that generate interactions above the controller bandwidth.

The cantilever deflection, which is proportional to the force error, is plotted in Fig. 7(c). From this figure it can be concluded that the standard controller results in significant imaging forces applied at points where abrupt changes in the sample occur. Such forces are intolerable when imaging sensitive or soft samples that can be damaged or deformed. The fast dual-stage controller ($\alpha = 10\,000$) reduces these force errors to a minimal amount and can be viewed as operating truly in constant-force mode. Further proof can be observed in Fig. 7(d) where a single line of the image is plotted. The low-pass characteristic of the slower controller is clearly evident.

In addition to improving the image quality, dual-stage control can also be used for increasing the imaging speed. However, with an integral controller, as speed is increased, the force error will increase proportionally. This trade-off is summarized approximately as follows:

$$\text{Speed increase} \times \text{Force error reduction} = 33 \qquad (19)$$

where 33 is the factor by which the bandwidth is increased and the other variables are the factors by which speed and force error are reduced or increased. That is, if the imaging speed is kept constant, the dual-stage controller allows a reduction of force error by 33 times. Conversely, if force error is constant, the dual-stage controller allows a 33 times improvement in imaging speed.

In Fig. 8 the imaging speed is doubled to 312 μm/s. The streaks in the standard controller image are due to the controllers inability to maintain probe contact after transient events like the repositioning of the probe at the beginning of each line. The higher gain of the dual-stage controller eliminates this problem. With maximum bandwidth, the dual-stage controller is able to reproduce the fine sample corrugations produced by the fabrication process.

VII. Conclusion

The piezoelectric tubes found in a scanning probe microscope have low resonance frequencies that severely limit the vertical feedback controller bandwidth. This imposes a strict limit on maximum imaging speed if large contact forces are to be avoided.

In this work, the vertical resonance frequency is vastly improved by retro-fitting a simple piezoelectric high-speed positioner. Due to the high stiffness and low mass, bandwidth can be increased by many times, 33 in this work.

To retain the large stroke developed by the tube scanner, a dual-stage configuration is adopted. In this configuration the fast, small perturbations experienced during imaging are provided by the high-speed positioner, while the slow, long-range travel is provided by the tube. This configuration retains the large stroke of the tube and the high resonance frequency of the high-speed stage.

Thanks to the increased resonance frequency, the dual-stage configuration allowed a 33 times increase in controller gain and closed-loop bandwidth. This translates to an image quality (force error) improvement of 33 times, or a speed increase of 33 times. Visually, the dual-stage controller eliminates image smearing and faithfully reproduces fine sample features that would otherwise be lost or distorted.

Future work includes improving the mechanical design of the high-speed positioner to increase the resonance frequency, load handling capability and range. More sophisticated controllers are also under development. These include positive position feedback controllers, integral resonance controllers, and model-based feed-forward controllers. Scope exists to increase the imaging speed by another order of magnitude.

References

[1] G. Binnig, H. Rohrer, C. Gerber, and E. Weibel, "Surface studies by scanning tunneling microscopy," *Phys. Rev. Lett.*, vol. 49, no. 1, pp. 57–61, 1982.

[2] G. Binnig, C. F. Quate, and C. Gerber, "Atomic force microscope," *Phys. Rev. Lett.*, vol. 56, no. 9, pp. 930–933, Mar. 1986.

[3] C. Gerber and H. P. Lang, "How the doors to the nanoworld were opened," *Nature Nanotechnol.*, vol. 1, no. 1, pp. 3–5, Oct. 2006.

[4] M. J. Brukman and D. A. Bonnell, "Probing physical properties at the nanoscale," *Phys. Today*, vol. 61, no. 6, pp. 36–42, Jun. 2008.

[5] Y. F. Dufrêne, "Towards nanomicrobiology using atomic force microscopy," *Nature Rev. Microbiol.*, vol. 6, pp. 674–680, Sep. 2008.

[6] N. Jalili and K. Laxminarayana, "A review of atomic force microscopy imaging systems: Application to molecular metrology and biological sciences," *Mechatronics*, vol. 14, no. 8, pp. 907–945, Oct. 2004.

[7] E. Meyer, H. J. Hug, and R. Bennewitz, *Scanning Probe Microscopy. The Lab on a Tip*. Heidelberg, Germany: Springer-Verlag, 2004.

[8] , B. Bhushan and H. Fuchs, Eds., *Applied Scanning Probe Methods (I-X)*. Heidelberg, Germany: Springer-Verlag, 2006.

[9] G. Btrrionetti, A. Bazzalia, and R. Orizio, "Atomic force microscopy: A powerful tool for surface defect and morphology inspection in semiconductor industry," *Eur. Phys. J. Appl. Phys.*, vol. 27, no. 1–3, pp. 101–106, Jul. 2004.

[10] A. Humphris, M. McConnell, and D. Catto, "A high-speed atomic force microscope capable of video-rate imaging," *Microscopy Anal.—SPM Supplement*, pp. 29–31, Mar. 2006.

[11] J. A. Vicary and M. J. Miles, "Pushing the boundaries of local oxidation nanolithography: Short timescales and high speeds," *Ultramicroscopy*, vol. 108, no. 10, pp. 1120–1123, Sep. 2008.

[12] A. Ferreira and C. Mavroidis, "Virtual reality and haptics for nanorobotics," *IEEE Robot. Autom. Mag.*, vol. 13, no. 3, pp. 78–92, Sep. 2006.

[13] A. A. Tseng, S. Jou, A. Notargiacomo, and T. P. Chen, "Recent developments in tip-based nanofabrication and its roadmap," *J. Nanosci. Nanotechnol.*, vol. 8, no. 5, pp. 2167–2186, May 2008.

[14] , A. A. Tseng, Ed., *Nanofabrication: Fundamentals and Applications*. Singapore: World Scientific, 2008.

[15] M. Guthold, X. Zhu, C. Rivetti, G. Yang, N. H. Thomson, S. Kasas, H. G. Hansma, B. Smith, P. K. Hansma, and C. Bustamante, "Direct observation of one-dimensional diffusion and transcription by escherichia coli RNA polymerase," *Biophys. J.*, vol. 77, no. 4, pp. 2284–2294, Oct. 1999.

[16] T. Ando, N. Kodera, T. Uchihashi, A. Miyagi, R. Nakakita, H. Yamashita, and K. Matada, "High-speed atomic force microscopy for capturing dynamic behavior of protein molecules at work," *e-J. Surface Sci. Nanotechnol.*, vol. 3, pp. 384–392, Dec. 2005.

[17] A. D. L. Humphris, M. J. Miles, and J. K. Hobbs, "A mechanical microscope: High-speed atomic force microscopy," *Appl. Phys. Lett.*, vol. 86, pp. 034 106(1)–034 106(3), 2005.

[18] G. Schitter, K. J. Åström, B. E. DeMartini, P. J. Thurner, K. L. Turner, and P. K. Hansma, "Design and modeling of a high-speed AFM-scanner," *IEEE Trans. Control Syst. Technol.*, vol. 15, no. 5, pp. 906–915, Sep. 2007.

[19] M. J. Rost, L. Crama, P. Schakel, E. van Tol, G. B. E. M. van Velzen Williams, C. F. Overgauw, H. ter Horst, H. Dekker, B. Okhuijsen, M. Seynen, A. Vijftigschild, P. Han, A. J. Katan, K. Schoots, R. Schumm, W. van Loo, T. H. Oosterkamp, and J. W. M. Frenken, "Scanning probe microscopes go video rate and beyond," *Rev. Scientific Instruments*, vol. 76, no. 5, pp. 053 710(1)–053 710(9), Apr. 2005.

[20] L. M. Picco, L. Bozec, A. Ulcinas, D. J. Engledew, M. Antognozzi, M. Horton, and M. J. Miles, "Breaking the speed limit with atomic force microscopy," *Nanotechnol.*, vol. 18, no. 4, pp. 044 030(1)–044 030(4), Jan. 2007.

[21] T. Sulchek, G. G. Yaralioglu, C. F. Quate, and S. C. Minne, "Characterization and optimization of scan speed for tapping-mode atomic force microscopy," *Rev. Scientific Instruments*, vol. 73, no. 8, pp. 2928–2936, 2002.

[22] S. Devasia, E. Eleftheriou, and S. O. R. Moheimani, "A survey of control issues in nanopositioning," *IEEE Trans. Control Syst. Technol.*, vol. 15, no. 5, pp. 802–823, Sep. 2007.

[23] S. O. R. Moheimani, "Accurate and fast nanopositioning with piezoelectric tube scanners: Emerging trends and future challenges," *Rev. Scientific Instruments*, vol. 79, no. 7, pp. 071 101(1)–071 101(11), Jul. 2008.

[24] T. Ando, "Control techniques in high-speed atomic force microscopy," in *Proc. Amer. Control Conf.*, Seattle, WA, Jun. 2008, pp. 3194–3200.

[25] D. Y. Abramovitch, S. B. Andersson, L. Y. Pao, and G. Schitter, "A tutorial on the mechanisms, dynamics, and control of atomic force microscopes," in *Proc. Amer. Control Conf.*, New York City, Jul. 2007, pp. 3488–3502.

[26] S. M. Salapaka and M. V. Salapaka, "Scanning probe microscopy," *IEEE Control Syst. Mag.*, vol. 28, no. 2, pp. 65–83, Apr. 2008.

[27] G. Schitter, "Improving the speed of AFM by mechatronic design and modern control methods," *Technisches Messen*, vol. 76, no. 5, pp. 266–273, May 2009.

[28] T. Ando, T. Uchihashi, and T. Fukuma, "High-speed atomic force microscopy for nano-visualization of dynamic biomolecular processes," *Progr. Surface Sci.*, vol. 83, no. 7–9, pp. 337–437, Nov. 2008.

[29] B. Rogers, T. Sulchek, K. Murray, D. York, M. Jones, L. Manning, S. Malekos, B. Beneschott, J. D. Adams, H. Cavazos, and S. C. Minne, "High speed tapping mode atomic force microscopy in liquid using an insulated piezoelectric cantilever," *Rev. Scientific Instruments*, vol. 74, no. 11, pp. 4683–4686, 2003.

[30] T. Sulchek, R. Hsieh, J. D. Adams, G. G. Yaralioglu, S. C. Minne, C. F. Quate, J. P. Cleveland, A. Atalar, and D. M. Adderton, "High-speed tapping mode imaging with active q control for atomic force microscopy," *Appl. Phys. Lett.*, vol. 76, no. 11, pp. 1473–1475, 2000.

[31] D. A. Walters, J. P. Cleveland, N. H. Thomson, P. K. Hansma, M. A. Wendman, G. Gurley, and V. Elings, "Short cantilevers for atomic force microscopy," *Rev. Scientific Instruments*, vol. 67, no. 10, pp. 3583–3590, 1996.

[32] K. K. Leang and A. J. Fleming, "High-speed serial-kinematic AFM scanner: Design and drive considerations," *Asian J. Control*, vol. 11, no. 2, pp. 144–153, Mar. 2009.

[33] A. J. Fleming and S. O. R. Moheimani, "Sensorless vibration suppression and scan compensation for piezoelectric tube nanopositioners," *IEEE Trans. Control Syst. Technol.*, vol. 14, no. 1, pp. 33–44, Jan. 2006.

[34] A. J. Fleming and K. K. Leang, "Charge drives for scanning probe microscope positioning stages," *Ultramicroscopy*, vol. 108, no. 12, pp. 1551–1557, Nov. 2008.

[35] A. J. Fleming and A. G. Wills, "Optimal periodic trajectories for band-limited systems," *IEEE Trans. Control Syst. Technol.*, vol. 13, no. 3, pp. 552–562, May 2009.

[36] T. Sulchek, S. C. Minne, J. D. Adams, D. A. Fletcher, A. Atalar, C. F. Quate, and D. M. Adderton, "Dual integrated actuators for extended range high speed atomic force microscopy," *Appl. Phys. Lett.*, vol. 75, no. 11, pp. 1637–1639, 1999.

[37] Y. Jeong, G. R. Jayanth, and C.-H. Menq, "Control of tip-to-sample distance in atomic force microscopy: A dual-actuator tip-motion control scheme," *Rev. Scientific Instruments*, vol. 78, no. 9, pp. 093 706(1)–093 706(7), 2007.

[38] T. Akiyama, U. Staufer, and N. F. de Rooij, "Atomic force microscopy using an integrated comb-shape electrostatic actuator for high-speed feedback motion," *Appl. Phys. Lett.*, vol. 76, no. 21, pp. 3139–3141, May 2000.

[39] Y. Yan, Y. Wu, Q. Zou, and C. Su, "An integrated approach to piezoactuator positioning in high-speed atomic force microscope imaging," *Rev. Scientific Instruments*, vol. 79, pp. 073 704(1)–073 704(9), Jul. 2008.

[40] G. Schitter, W. F. Rijkée, and N. Phan, "Dual actuation for high-bandwidth nanopositioning," in *Proc. IEEE Conf. Decision Control*, Cancun, Mexico, Dec. 2008, pp. 5176–5181.

[41] J. Maess, A. J. Fleming, and F. Allgöwer, "Simulation of dynamics-coupling in piezoelectric tube scanners by reduced order finite element models," *Rev. Scientific Instruments*, vol. 79, pp. 015 105(1)–015 105(9), Jan. 2008.

[42] S. A. Z. Jahromi, M. Salomons, Q. Sun, and R. A. Wolkow, "Prediction of the resonant frequency of piezoelectric tube scanners through three-dimensional finite element modeling of a tube assembly," *Rev. Scientific Instruments*, vol. 79, no. 7, pp. 076 104(1)–076 104(3), Jul. 2008.

[43] C. J. Chen, "Electromechanical deflections of piezoelectric tubes with quartered electrodes," *Appl. Phys. Lett.*, vol. 60, no. 1, pp. 132–134, Jan. 1992.

[44] A. A. Mamun, I. Mareels, T. H. Lee, and A. Tay, "Dual stage actuator control in hard disk drive—A review," in *Proc. Ann. Conf. IEEE Ind. Electron. Soc.*, Roanoke, VA, Nov. 2003, vol. 3, pp. 2132–2137.

Andrew J. Fleming was born in Dingwall, Scotland, in 1977. He received the Bachelor's degree in electrical engineering and the Ph.D. degree from The University of Newcastle, Callaghan, Australia, in 2000 and 2004, respectively.

He is currently an Australian Research Council Fellow with the School of Electrical Engineering and Computer Science, The University of Newcastle. His research interests include nano-positioning, high-speed scanning probe microscopy, micro-cantilever sensors, and sensor-less control of sound and vibration. He is the coauthor of two books, several patent applications, and more than 80 Journal and conference papers.

Dr. Fleming was a recipient of the University of Newcastle Vice-Chancellors Award for Researcher of the Year, the Faculty of Engineering and Built Environment Award for Research Excellence, and the IEEE Control Systems Society Outstanding Paper Award for research published in the IEEE TRANSACTIONS ON CONTROL SYSTEMS TECHNOLOGY, all in 2007. He is an Associate Editor of *Advances in Acoustics and Vibration*.